Indium hydroxide/silver/carbon nanocomposite: Synthesis via galvanic reaction between In nanoparticles and silver nitrate, characterization and its photocatalytic activity

Pui Munn Wong[1, a], Teck Hock Lim[1,b*] Joon Ching Juan[2,c] and Jau Choy Lai[3,d]

[1]Faculty of Applied Sciences, Tunku Abdul Rahman University College, 53300, Kuala Lumpur, Malaysia

[2]Nanotechnology & Catalysis Research Centre, University of Malaya, 50603, Kuala Lumpur, Malaysia

[3]Faculty of Chemical & Energy Engineering, Universiti Teknologi Malaysia, 81310, Skudai, Johor, Malaysia

[a]wongpm-wa13@student.tarc.edu.my, [b]limth@tarc.edu.my, [c]jcjuan@um.edu.my, [d]jclai@cheme.utm.my

Keywords: galvanic replacement, indium nanoparticles, $In(OH)_3$/Ag/C nanocomposite, photodegradation, methylene blue

Abstract: Sub-10 nm indium metal nanoparticles (In NPs) stabilized on conductive carbon were reacted with silver nitrate in dark in water at room temperature in a galvanic replacement manner to produce indium hydroxide/silver/carbon nanocomposite (In(OH)3/Ag/C). The chosen carbon imparted colloidal stability, high surface area and water dispersibility suitable for photodegradation of harmful dyes in water. The size and shape of indium hydroxide and silver nanoparticles produced were found to be similar to that of the In NPs started with. The nanocomposite was characterized by Transmission Electron Microscopy (TEM), Energy Dispersive X-ray Spectroscopy (EDAX), Powder X-Ray Diffraction (PXRD) and Thermogravimetric Analysis (TGA). The galvanic reaction between In NPs and silver nitrate was tracked with UV-Vis Spectroscopy in a control experiment without conducting carbon to confirm that the reaction was indeed thermodynamically spontaneous as indicated by the positive electromotive force (EMF) of +1.14 V calculated for In/Ag+ redox couple. The nanocomposite's photocatalytic performance was evaluated to be circa 90% under UVC radiation when 10 ppm of methylene blue and 13 wt% of indium hydroxide/silver loading on carbon were used.

Introduction

Nanoparticles (NPs) exhibit size and shape dependent chemical and physical properties not found in their bulk counterparts [1-5]. A combination of high surface area and high surface energy renders them excellent candidates for a wide range of technological applications in the fields of optoelectronics, healthcare, catalysis and hazardous waste degradation [6-12]. Through the joint effort of many researchers, the field of nanoscience and nanotechnology has advanced considerably and its importance in environmental applications is gaining the attention of researchers and governmental bodies worldwide [13-16].

In terms of nanoparticle design and synthesis, liquid or solution based methods have become more popular recently due to the possibility to scale up more readily, specifically when the reactions could be carried out under ambient conditions [17-18]. Amongst the methods developed to produce nanoparticles in solution, galvanic reactions between metallic nanoparticles and metal ions have been proven as a versatile approach from which a wide range of nanoparticles, ranging from AgPd, AgPt, AuCu nanoalloys and hollow AgAu nanocages could be engineered [19-21].

While from the standard reduction potentials one could estimate whether a galvanic reaction would occur in terms of thermodynamics, the mechanism and kinetics of the galvanic reaction of interest are often uncertain or elusive. For example, while AgAu nanocages were reported in the year 2006, the actual mechanism for the reaction was only confirmed in the year 2017 by Moreau et al [22].

Galvanic reactions may not always lead to the formation of alloys and hollow structures. For example, Kumar et al. found that solid Au NPs could be prepared directly on a cationic exchange membrane via a 50% replacement of Ag NPs with gold trichloride ($AuCl_3$) [23].

Research work related to galvanic reactions has primarily been focused on noble metal systems and In NPs have received little attention [19-23]. This is likely due to that In NPs are less readily available and have to be synthesized under more stringent conditions, including removal of oxygen and moisture from the synthetic system [24].

The standard reduction potential for Ag^+/Ag redox pair (0.8 V versus standard hydrogen electrode (SHE)) is higher than that of In^{3+}/In redox pair (-0.34 vs SHE) [25,26]. The electromotive force of the In/Ag^+ redox pair therefore could be calculated as +1.14 V, indicating a thermodynamically spontaneous reaction.

To the best of the authors' knowledge, the galvanic reactions between In NPs and metal salts such as silver nitrate ($AgNO_3$) and gold chloride have not been previously reported. Herein, we report the galvanic reaction between In NPs and $AgNO_3$ in ethanol and in a confined space (i.e. water saturated carbon paste). The confined-space approach was designed to synthesize $In(OH)_3$/Ag/C nanocomposite with uniform size and shape via immobilizing In NPs, $In(OH)_3$ and Ag NPs on carbon. The photocatalytic performance of the nanocomposite was evaluated using methylene blue at three different concentrations under UVC at room temperature.

Experimental Section

Materials

Unless otherwise mentioned, analytical reagent (AR) grade chemicals were used. Trioctylphosphine oxide (TOPO, tech. 90%), isobutylamine (98%), indium trichloride anhydrous ($InCl_3$; 99.995%), lithium borohydride ($LiBH_4$; 4M in THF) and sodium borohydride ($NaBH_4$; 98+%) were purchased from ACROS Organics. Super P conductive carbon black (99+%) was purchased from Alfa Aesar. Ethyl alcohol (99.8%) and silver nitrate ($AgNO_3$; 99%) were purchased from Systerm. Methylene blue (C.I 52015) was purchased from ChemSoln. Methanol was purchased from Merck. Fresh double-distilled water was used. All chemicals were used as received. Air-sensitive synthesis was carried out under high purity Ar gas using standard Schlenk techniques and workup procedures were performed in air.

Preparation of indium nanoparticles (In NPs)

In NPs were synthesized using a literature method reported by Lim et al [24]. Briefly, 0.17 g of $InCl_3$ was dissolved in 20 ml of isobutylamine in which 0.50 of TOPO was first dissolved in. Three mole equivalent of $LiBH_4$ in THF was added dropwise to the mixture during which bubbles were observed. The mixture was heated to gentle reflux for 15 minutes during which the transparent colourless solution changed from bright yellow to dark brown and finally black in colour. The product was diluted with ethanol and centrifuged at 1000 rpm at room temperature to isolate In NPs as a dark brown pellet/precipitate.

Preparation of In NPs dispersed on conducting carbon (In NPs/C).

The dark brown precipitate from section 2.1.1 was dispersed on 0.20 g of Super P conducting carbon in ethanol via sonication for 3 minutes. The suspension was then purged with a gentle stream of N_2 gas to yield dried In NPs/C.

Synthesis of indium hydroxide/silver/conducting carbon nanocomposite ($In(OH)_3$/Ag/C)

0.10 g of Super P carbon was found capable of absorbing a maximum of 1.5 ml of water to form a paste without phase separation. This ratio was followed for the $In(OH)_3$/Ag/C nanocomposite preparation. Dried In NPs/C was saturated with freshly prepared aqueous $AgNO_3$ (45 mM) to produce a paste. The paste was left in dark at 25˚C for 24 hours for the galvanic reaction between In NPs and $AgNO_3$ to occur. An In:Ag ratio of 1.5:1 was used since one In atom would be able to reduce three Ag^+ ions before forming an In^{3+} ion. A fraction of the In NPs reacted with $AgNO_3$ to yield Ag NPs and the rest reacted with water to form $In(OH)_3$ NPs. The product was washed with water under vacuum suction. The colourless filtrate was tested with excess freshly prepared aqueous $NaBH_4$. No brown colour developed after the $NaBH_4$ treatment, indicating all $AgNO_3$ has been retained in the nanocomposite.

Characterization

UV-VIS absorption spectroscopy

The UV-Vis measurements were performed on a Hitachi UH5300 spectrophotometer with a scan range of 200 nm-1000 nm and a scan speed of 800 nm/min. The solution was filtered over syringe filter (0.2 μm) to produce a transparent sample prior to UV-VIS measurement.

Differential scanning calorimetry-thermogravimetric analysis (DSC-TGA)

DSC-TGA was conducted using a SDT Q600 from TA Instruments using air and an alumina sample holder. The heating rate was set as 10˚C/min and the sample was heated from 25 to 1000 ˚C. The flow rate of air was 100 mL/min.

Powder X-ray diffraction (PXRD)

A PANalytic Empyrean X-Ray diffractometer with Cu Kα (λ= 1.5404 Å) operating at 45 kV, 40 mA and 25˚C was used to carry out phase identification. The scanning range was 20.00-70.00˚, step size was 0.0260 ˚2θ and scan speed was 2˚/min.

Transmission electron microscopy (TEM)/Energy dispersive X-ray spectroscopy (EDAX)

Bright field TEM images were obtained using a Hitachi HT-7700 operating at 120.0 kV. Samples were sonicated and dispersed on lacey carbon films on copper grids prior to studies. The elemental composition of sample was determined with a Bruker XFlash 6T|60 Detector at 120.0 kV.

Galvanic reaction In NPs and $AgNO_3$

In NPs pellet prepared (see section 2.1.1) was dispersed in 50 ml of ethanol. 0.5 mL of $AgNO_3$ (0.135 M) was injected into the mixture, mixed well for 30 seconds and 3 ml was taken and placed in a quartz cuvette for tracking the reaction using UV-VIS spectroscopy for 2 hours. 50 ml of ethanol is required to dilute the reactant such that it could be tracked directly with UV-Vis spectrophotometer without further dilution.

Methylene blue removal and photocatalytic performance of $In(OH)_3$/Ag/C

Photodegradation of methylene blue dye was carried out in a photoreactor with a UVC light source operating at 15 W. 25 mg of $In(OH)_3$/Ag/C was dispersed in 80 ml of methylene blue

solution (freshly prepared at 25 ppm, 10 ppm and 5 ppm) via sonication. The mixture became uniformly black. No precipitation/separation over the 6-hour study was observed, signifying that a stable suspension was obtained. With constant stirring at 100 rpm, an absorption equilibrium in dark was first allowed to establish over 3 hours, followed by 3-hour of exposure to UVC to confirm the photocatalytic activity of $In(OH)_3$/Ag/C. The changes in absorbance at 664 nm were followed using a UV-Vis spectrophotometer because methylene blue displayed an absorption maximum at 664 nm.

Results and Discussions

Galvanic reaction between In NPs and $AgNO_3$ in ethanol

From published values of standard reduction potentials (see Introduction), the electromotive force calculated for the In/Ag^+ redox system was +1.14 V [25-26]. This indicates a thermodynamically spontaneous reaction. To avoid a second reaction where In NPs would react with water to form $In(OH)_3$, the galvanic reaction between In NPs and $AgNO_3$ was carried out in ethanol in order to confirm the reaction would take place. The reaction also served to gauge whether Ag NPs could be produced by studying the development of a new absorption maximum in the UV-VIS spectrum of the product obtained after 2 hours of reaction.

Galvanic reaction is known in literature as an effective means to produce nanoparticles where good controls in chemical composition, size and shape could be achieved simultaneously. Synthetic parameters such as concentration, pH value, size of reactant nanoparticles, temperature and the intrinsic diffusion coefficients of atoms are among the few key parameters [27-32].

Figure 1 showed the UV-Vis absorption spectrum of In NPs in ethanol alone and that after the treatment with $AgNO_3$ at 25 ^oC for 2 hours. In NPs did not show a strong absorption in the visible region and this observation is consistent with literature reports [24, 33]. The product obtained after 2-hour of galvanic reaction however absorbed strongly at 442 nm. This explained the much stronger brown colour observed for the product (top right hand corner of Figure 1).

The presence of 442 nm absorption was attributed to the plasmon resonance of Ag NPs (20-40 nm in diameter) commonly observed in literature reports [34-35]. The relatively broad full-width-half-maximum (FWHM) of the absorption peak at 442 nm suggested that the size of the Ag NPs was not uniform. Non-uniformity in size is not ideal for photocatalytic applications especially when the chemical properties of nanoparticles are size dependent.

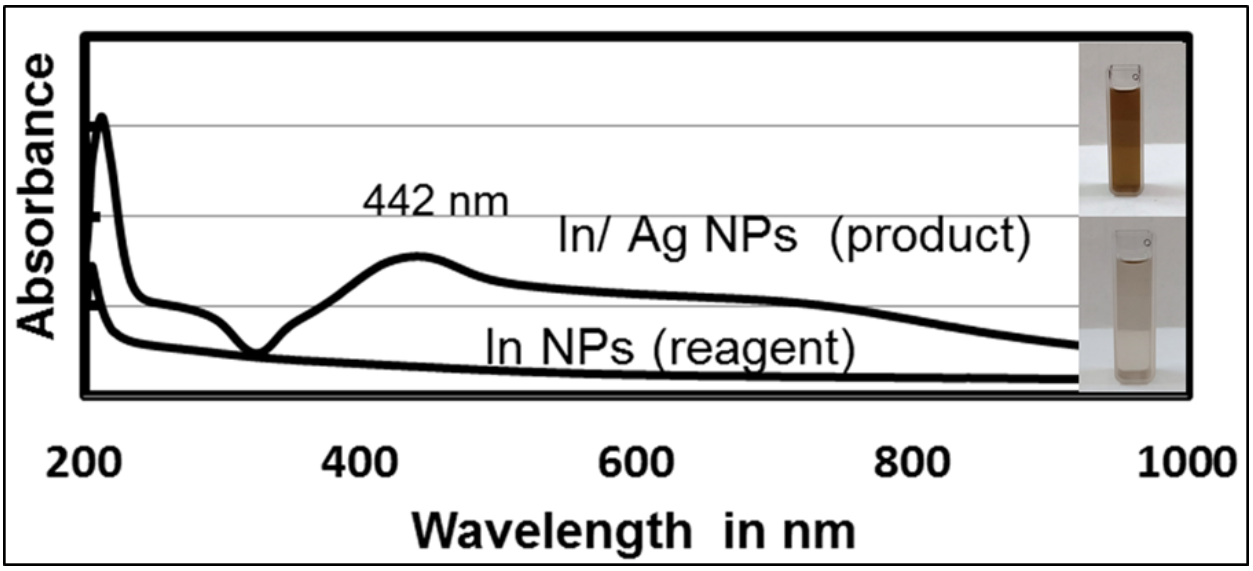

Fig. 1: UV-Vis absorption of as-synthesized In NPs in ethanol and a mixture of Ag NPs/In NPs after a 2-hour galvanic reaction between In NPs and $AgNO_3$. Significantly more intense brown colour was observed for the product, consistent with the development of the new absorption maximum at 442 nm.

Preparation of $In(OH)_3$/Ag/C composite

For catalysis, we aimed to produce Ag NPs of uniform size and lesser than 10 nm in diameter in order to enhance catalytic activity [36-38]. Based on the discussion in Section 3.1, the galvanic reaction in ethanol appeared to produce polydispersed Ag NPs. Therefore the Ag NPS produced via galvanic reaction must be further stabilized and prevented from growing bigger in size. To achieve this, we devised a method where sub-10 nm In NPs were first dispersed on conductive carbon to produce In NPs/C composite.

In NPs/C allowed the galvanic reaction with $AgNO_3$ to be conducted in a confined manner when the amount of water was controlled such that it would just saturate the carbon without overflowing or phase separation. This was to ensure the galvanic reaction could only take place locally where sub-10 nm In NPs would produce sub-10 nm Ag NPs. When the reactive In NPs were fixed on highly absorbing carbon, it was expected that the movement of In NPs in the solution due to Brownian motion was significantly deterred with particles immobilized on the surface of the porous carbon substrate [39-40]. This helped prevent agglomeration, leading to uniform sub-10 nm $In(OH)_3$ NPs and Ag NPs.

Figure 2 describes the preparation of $In(OH)_3$/Ag/C in more details. The galvanic reaction between In NPs and $AgNO_3$ was carried out in dark to avoid reduction of $AgNO_3$ by ambient light. After 24 hours, the product was washed with water and the filtrate was treated with excess aqueous $NaBH_4$. A clear colourless product showed that all $AgNO_3$ had reacted.

In a control experiment where conducting carbon alone was treated with $AgNO_3$ for 24 hours, the filtrate turned intensely brown after the addition of $NaBH_4$. This showed that most of the $AgNO_3$ has been washed out from the carbon as they have no In NPs to react with (See Supporting information S1).

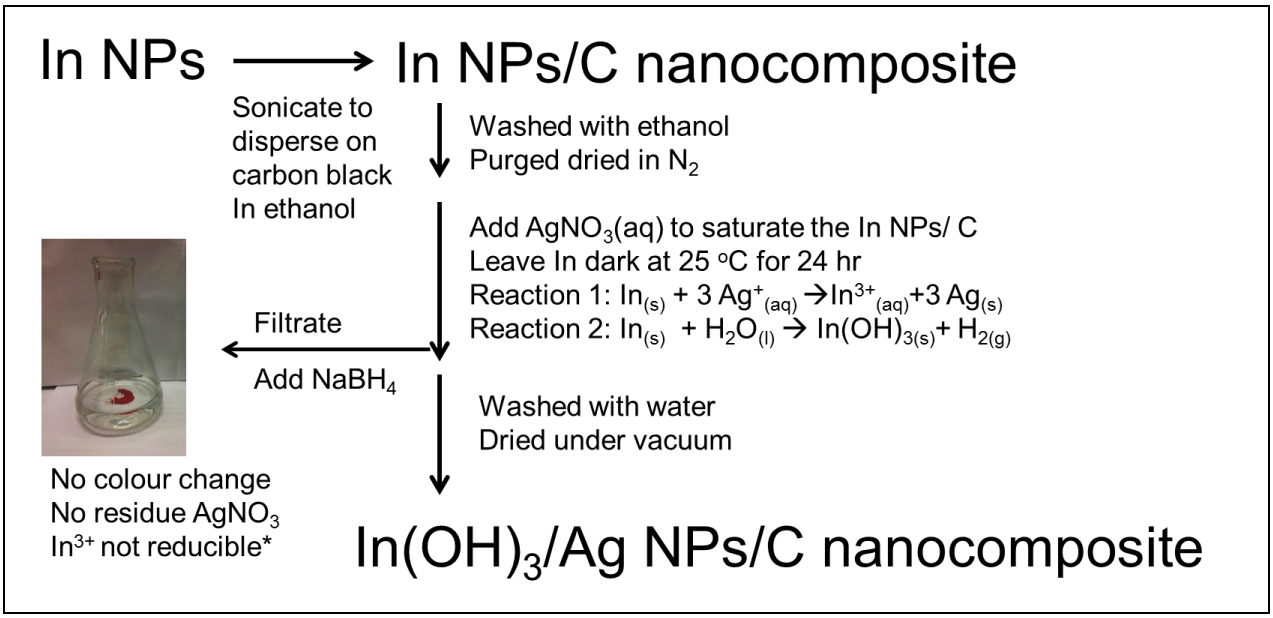

Fig. 2: Schematic flow chart for the preparation of $In(OH)_3$/Ag NPs/C nanocomposite. Any residue $AgNO_3$ would be reduced to brown/black Ag particles. Colourless filtrate after 24 hours in dark indicated all $AgNO_3$ had reacted. Note: $In^{3+}_{(aq)}$ is not reducible by $NaBH_4$ in air in water.

Morphological and structural characterization

Figure 3 showed the PXRD diffractogram obtained for the $In(OH)_3$/Ag/C nanocomposite. All three components were present with the $In(OH)_3$ phase matched to dzhalindite (ICDD: 98-003-5637) and Ag phase matched to FCC Ag (ICDD: 98-006-5995). The broad peak at 20 $^{o}(2\theta)$ is characteristic of amorphous carbon. This observation is consistent with the PXRD pattern reported for Super P conducting carbon [41].

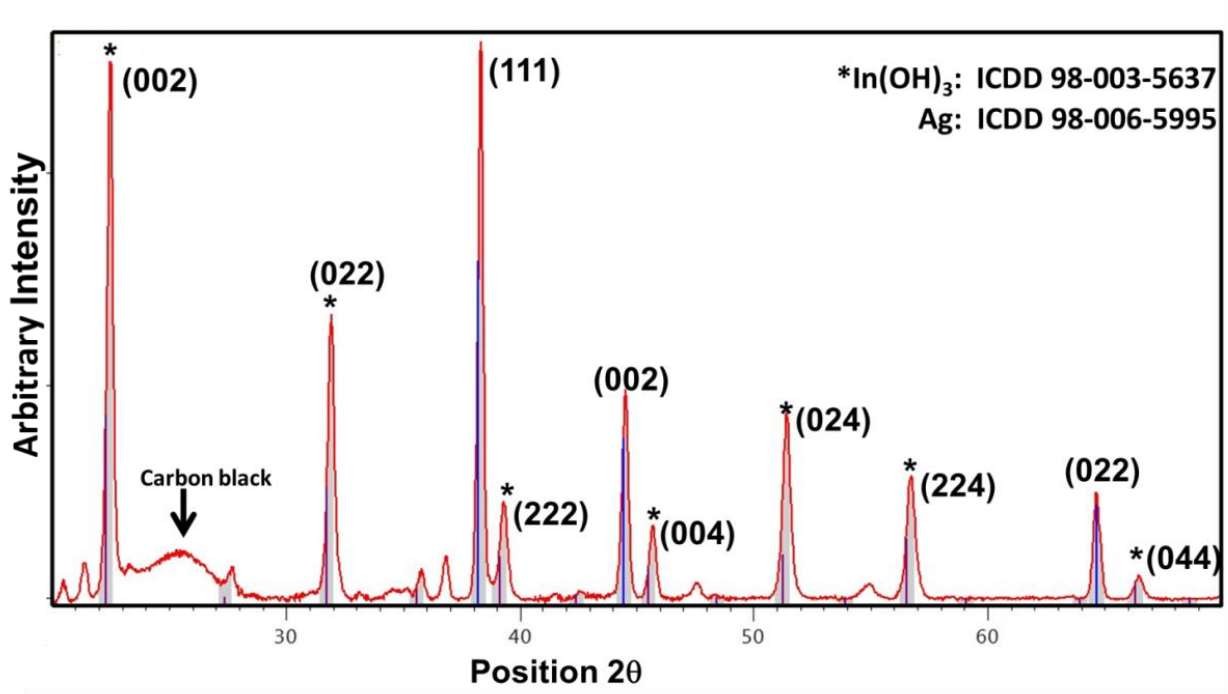

Fig. 3: PXRD diffractogram of $In(OH)_3$/Ag/C nanocomposite. Highly crystalline $In(OH)_3$ (marked by asterisk) and Ag were present and the broad diffraction at 20 ^{o} was attributed to carbon as described in literature [41].

Figure 4(a) and 4(b) showed sub-10 nm nanoparticles well-dispersed on conducting carbon substrate. The particle size of $In(OH)_3$ NPs and Ag NPs appeared to be similar. The particles were found to be uniform with an average diameter of 6.6±0.9 nm (see Supporting information S2). Different contrasts could be observed for the particles decorating the carbon substrate. The differences in contrast alone however did not allow us to directly distinguish Ag NPs from $In(OH)_3$ NPs due to the influence of carbon substrate during TEM imaging. EDAX analysis of the $In(OH)_3$/Ag/C nanocomposite revealed the presence of Ag, In, O and C (see Figure 4(c)).

The average diameter of 6.6±0.9 nm determined for $In(OH)_3$ and Ag NPs is very close to the 7 nm reported for In NPs produced by Lim et al.[24] This indicated that the confined space approach (see last paragraph of Introduction) devised did work to facilitate particle size control as hypothesised.

In the absence of In NPs, treatment of carbon with $AgNO_3$ overnight, did not lead to production of Ag NPs decorated carbon (see Supporting information Figure S3). Few nanoparticles were observed and these were attributed to the absorbed $AgNO_3$ which decomposed to form Ag NPs under electron beam during TEM analysis. Electron beam induced formation of Ag NPs from $AgNO_3$ has been documented in literature [42].

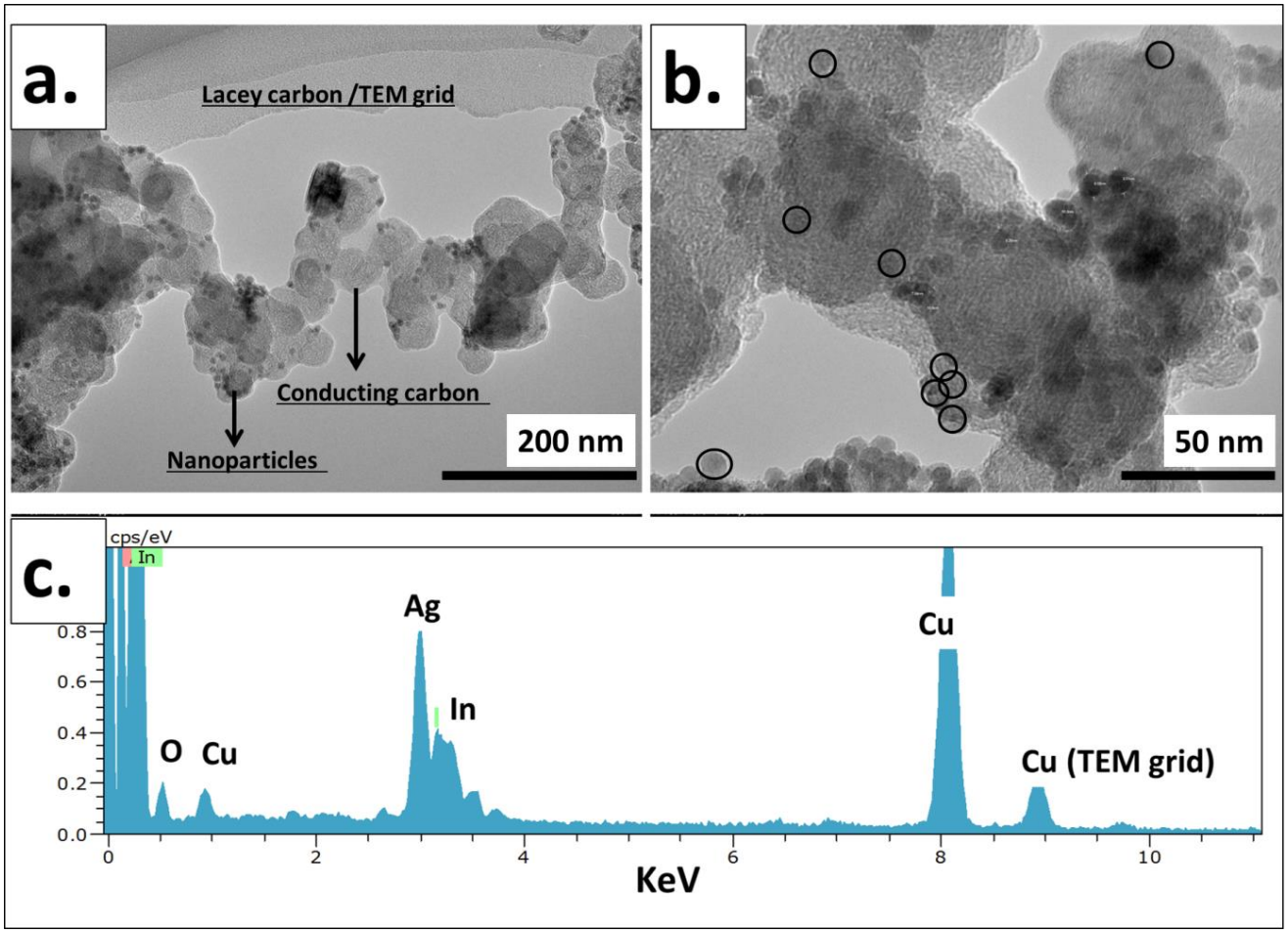

Fig. 4: TEM and EDAX analysis of $In(OH)_3$/Ag/C nanocomposite. (a) A bright field TEM image shows nanoparticles well-dispersed on carbon substrate; (b) The nanoparticle appeared to be uniform in size with an average size of 6.6±0.9 nm. Ag NPs are expected to exhibit a higher contrast than $In(OH)_3$ under bright field conditions; (c) EDAX analysis shows the presence of Ag, In, O and Cu. The copper signals originated from the copper/lacey carbon grid.

$In(OH)_3$/Ag/C as Photocatalyst for Methylene Blue's Removal

$In(OH)_3$/Ag/C nanocomposite produced was tested as photocatalyst for the removal of methylene blue. $In(OH)_3$/Ag/C was dispersed into a freshly prepared methylene blue solution and an absorption equilibrium in dark was allowed to occur before switching on the UVC light.

As may be observed in Figure 5, UVC light alone could only degrade 15 % of methylene blue after 6 hours. In the presence of $In(OH)_3$/Ag/C photocatalyst, a significant improvement in methylene blue removal efficiency was observed. The effect of the photocatalyst was noteworthy because a mere 3.2 mg of $In(OH)_3$/Ag NPs present on the carbon (total 25 mg $In(OH)_3$/Ag/C loading) was able to enhance the degradation from 15 % to 40 % in 80 ml of 25 ppm methylene blue solution.

Effect of concentration of methylene blue.

Figure 5 compared the removal of methylene blue using 25 mg of $In(OH)_3$/Ag/C (3.2 mg $In(OH)_3$/Ag NPs equivalent) for 80 ml of solution over 6 hours under mild UVC irradiation with constant stirring across three methylene blue concentrations.

At 10 ppm concentration, the catalyst absorbed circa half of the methylene blue present in dark within 3 hours. After UVC-light was turned on, a significant drop in methylene blue concentration was observed within the first hour. This signifies a significant synergistic effect of absorption by conducting carbon coupled to the photocatalytic activity endowed by the $In(OH)_3$/Ag NPs moiety of the nanocomposite. An overall 88% removal efficiency was achieved within 6 hours under mild UVC.

Molecules of methylene blue absorbed on carbon were closer to the surface of $In(OH)_3$/ Ag NPs photocatalyst. Exposure to UVC light led to the formation of electron-hole pair which helped degrade methylene blue. The conductive nature of the carbon may have allowed a more effective charge separation, leading to an enhanced the photocatalytic performance of In(OH)3/Ag/C as observed in other photocatalytic systems [43].

A lower removal efficiency of 40% was detected when 25 ppm of methylene blue was used. The declining slope of the graph however indicated that given sufficient time a higher removal efficiency would be possible. By reducing the concentration of methylene blue to 5 ppm, a complete absorption in dark within the first 3 hours could be achieved and no photocatalytic activity could be directly detected after UVC-light was switched on.

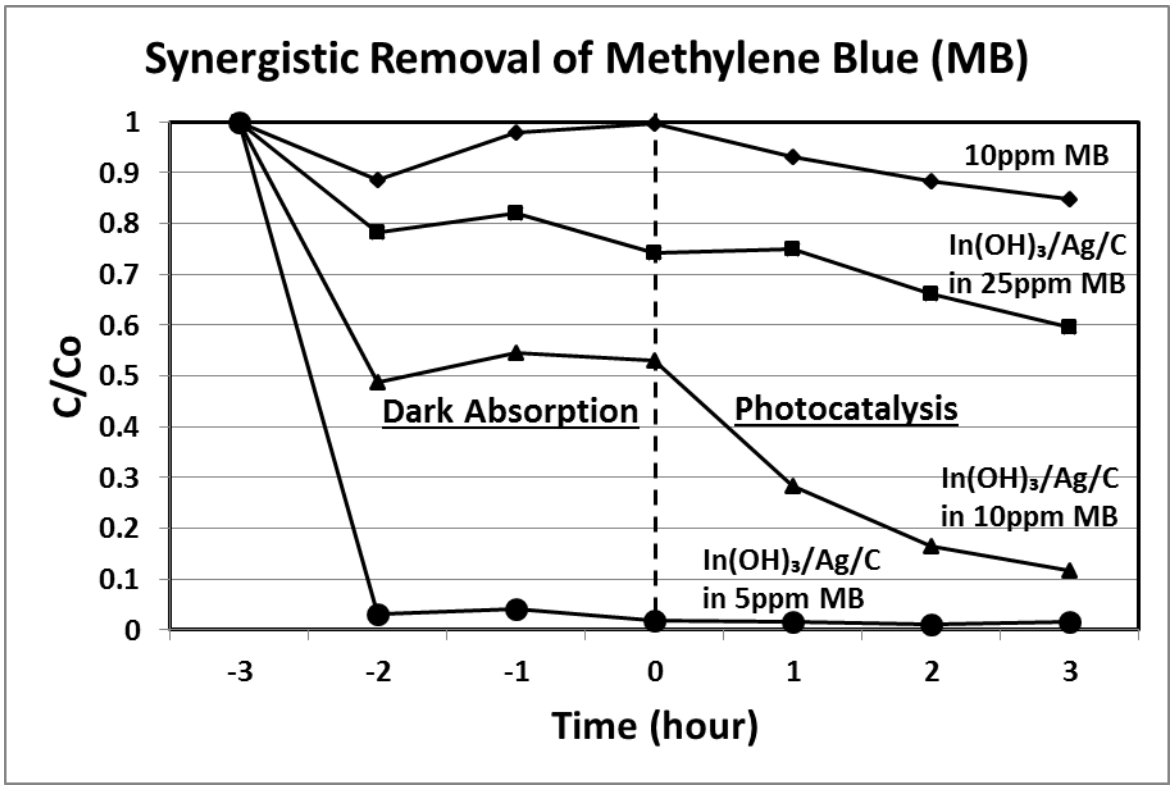

Fig. 5: Removal of methylene blue in water using 25 mg $In(OH)_3$/Ag/C at three different MB concentrations. The volume of MB solution tested was fixed at 80 ml. At 10 ppm, an overall 88% removal efficiency was achieved. At 5 ppm, $In(OH)_3$/Ag/C absorbed all methylene blue present.

Conclusion

An $In(OH)_3$/Ag/C nanocomposite was successfully produced and characterized. The nanocomposite was prepared from a controlled galvanic reaction between In NPs/C and aqueous $AgNO_3$ in dark at room temperature for 24 hours. The amount of water used was minimal such that a saturated carbon paste was obtained. The carbon immobilized the In NPs. Mobile Ag^+ in water reacted with a fraction of the In NPs to form Ag NPs. The rest reacted with water to form $In(OH)_3$ NPs. The Ag and $In(OH)_3$ NPs produced were found to be spherical in shape with an average diameter of 6.6±0.9 nm, similar to the size of In NPs started with. At 10 ppm methylene blue concentration, the nanocomposite exhibited its best photocatalytic degradation performance with a ~90% overall removal efficiency achieved in 6 hours under a mild 15W UVC with a 25 mg $In(OH)_3$/Ag/C loading.

References

[1] C. Xia, W. Wu, T. Yu, X. Xie, C. van Oversteeg, H.C. Gerritsen, C. de Mello Donega, Size-dependent band-gap and molar absorption coefficients of colloidal CuInS2 quantum dots, ACS Nano 12 (2018) 8350-8361.

[2] D.V. Talapin and E.V. Shevchenko, Introduction: nanoparticle chemistry, Chem. Rev. 116 (2016) 10343-10345.

[3] N.T.K. Thanh, N. Maclean and S. Mahiddine, Mechanisms of nucleation and growth of nanoparticles in solution, Chem. Rev. 114 (2014) 7610-7630.

[4] N. Fischer, B. Clapham, T. Feltes, E. van Steen and M. Claeys, Size-dependent phase transformation of catalytically active nanoparticles captured in situ, Angew. Chem. 126 (2014) 1366-1369.

[5] V.H. Grassian, When size really matters: size-dependent properties and surface chemistry of metal and metal oxide nanoparticles in gas and liquid phase environments, J. Phys. Chem. C 112 (2008) 18303-18313.

[6] X. Han, K. Xu, O. Taratula and K. Farsad, Applications of nanoparticles in biomedical imaging, Nanoscale 11 (2019) 799-819.

[7] R. Chen, J. Cao, Y. Duan, Y. Hui, T.T. Chuong, D. Ou, F. Han, F. Cheng, X. Huang, B. Wu, N. Zheng, High-efficiency, hysteresis-less, uv-stable perovskite solar cells with cascade ZnO–ZnS electron transport layer, J. Am. Chem. Soc. 141 (2018) 541-547.

[8] N. Dwivedi, S. Kumar, J.D. Carey and C. Dhand, Functional nanomaterials for electronics, optoelectronics, and bioelectronics, Journal of Nanomaterials 2015 (2015) 1-2.

[9] W.J. Stark, P.R. Stoessel, W. Wohlleben and A. Hafner, Industrial applications of nanoparticles, Chem. Soc. Rev. 44 (2015) 5793-5805.

[10] N. Sharma, H. Ojha, A. Bharadwaj, D.P. Pathak and R.K. Sharma, Preparation and catalytic applications of nanomaterials: a review, RSC Adv. 5 (2015) 53381-53403.

[11] Y. Xia, H. Yang and C.T. Campbell, Nanoparticles for catalysis, Accounts of Chemical Research 46 (2013) 1671-1672.

[12] R. Ferrando, J. Jellinek and R.L. Johnston, Nanoalloys: from theory to applications of alloy clusters and nanoparticles, Chem. Rev. 108 (2008) 845-910.

[13] R.K. Ibrahim, M. Hayyan, M.A. AlSaadi, A. Hayyan and S. Ibrahim, Environmental application of nanotechnology: air, soil, and water, Environ. Sci. Pollut. Res. 23 (2016) 13754-13788.

[14] S. Das, B. Sen and N. Debnath, Recent trends in nanomaterials applications in environmental monitoring and remediation, Environ. Sci. Pollut. Res. 22 (2015) 18333-18344.

[15] A. De Luca and B.B. Ferrer, Nanomaterials for water remediation: synthesis, application and environmental fate, in: G. Lofrano, G. Libralato and J. Brown (Eds.), Nanotechnologies for Environmental Remediation, Springer Nature, Cham, 2017, pp. 25-60.

[16] P. Singh, A. Ojha, A. Borthakur, R. Singh, D. Lahiry, D. Tiwary and P.K. Mishra, Emerging trends in photodegradation of petrochemical wastes: a review, Environ. Sci. Pollut. Res. 23 (2016) 22340-22364.

[17] L.G. AbdulHalim, S. Ashraf, K. Katsiev, A.R. Kirmani, N. Kothalawala, D.H. Anjum, S. Abbas, A. Amassian, F. Stellacci, A. Dass, I. Hussain and O.M. Bakr, A scalable synthesis of highly stable and water dispersible Ag44(SR)30 nanoclusters, J. Mater. Chem. A 1 (2013) 10148-10154.

[18] C.J. Tighe, R.Q. Cabrera, R.I. Gruar and J.A. Darr, Scale up production of nanoparticles: continuous supercritical water synthesis of Ce–Zn oxides, Ind. Eng. Chem. Res. 52 (2013) 5522-5528.

[19] S.E. Skrabalak, L. Au, X. Li and Y. Xia, Facile synthesis of Ag nanocubes and Au nanocages, Nat. Protoc. 2 (2007) 2182-2190.

[20] X. Liu and D. Astruc, From galvanic to anti-galvanic synthesis of bimetallic nanoparticles and applications in catalysis, sensing, and materials science, Adv. Mater. 29 (2017) 1605305.

[21] L.M. Moreau, C.A. Schurman, S. Kewalramani, M.M. Shahjamali, C.A. Mirkin and M.J. Bedzyk, How Ag nanospheres are transformed into AgAu nanocages, J. Am. Chem. Soc. 139 (2017) 12291-12298.

[22] Z. Jiang, Q. Zhang, C. Zong, B. Liu, B. Ren, Z. Xie and L. Zheng, Cu–Au alloy nanotubes with five-fold twinned structure and their application in surface-enhanced Raman scattering, J. Mater. Chem. 22 (2012) 18192-18197.

[23] R. Kumar, A.K. Pandey, S. Das, S. Dhara, N.L. Misra, R. Shukla, A.K. Tyagi, S.V. Ramagiri, J.R. Bellare and A. Goswami, Galvanic reactions involving silver nanoparticles embedded in cation-exchange membrane, ChemComm 46 (2010) 6371-6373.

[24] T.H. Lim, B. Ingham, K.H. Kamarudin, P.G. Etchegoin and R.D. Tilley, Solution synthesis of monodisperse indium nanoparticles and highly faceted indium polyhedra, Cryst. Growth Des. 10 (2010) 3854-3858.

[25] S. Trasatti, The absolute electrode potential: an explanatory note (Recommendations 1986), Pure Appl. Chem. 58 (1986) 955-966.

[26] A.K. Covington, M.A. Hakeem and W.F.K. Wynne-Jones, 842. Standard potential of the In|In3+ electrode, J. Chem. Soc. (Resumed) 0 (1963) 4394-4401.

[27] A.N. Chen, S.M. McClain, S.D. House, J.C. Yang and S.E. Skrabalak, Mechanistic study of galvanic replacement of chemically heterogeneous templates, Chem. Mater. 31 (2019) 1344-1351.

[28] G.G. Li, M. Sun, E. Villarreal, S. Pandey, S.R. Phillpot and H. Wang, Galvanic replacement-driven transformations of atomically intermixed bimetallic colloidal nanocrystals: effects of compositional stoichiometry and structural ordering, Langmuir 34 (2018) 4340-4350.

[29] G. Zhou, H. Wang, J. Tian, Y. Pei, K. Fan, M. Qiao, B. Sun and B. Zong, Ru-Zn/ZrO2 nanocomposite catalysts fabricated by galvanic replacement for benzene partial hydrogenation, ChemCatChem 10 (2017) 1184-1191.

[30] K. Niu, S.A. Kulinich, J. Yang, A.L. Zhu and X. Du, Galvanic replacement reactions of active-metal nanoparticles, Chem. Eur. J. 18 (2012) 4234-4241.

[31] Y. Sun and Y. Wang, Monitoring of galvanic replacement reaction between silver nanowires and HAuCl4 by in situ transmission X-ray microscopy, Nano Lett. 11 (2011) 4386-4392.

[32] J. Chen, B. Wiley, J. McLellan, Y. Xiong, Z. Li and Y. Xia, Optical properties of Pd−Ag and Pt−Ag nanoboxes synthesized via galvanic replacement reactions, Nano Lett. 5 (2005) 2058-2062.

[33] Y. Zhao, Z. Zhang and H. Dang, A novel solution route for preparing indium nanoparticles, J. Phys. Chem. B 107 (2003) 7574-7576.

[34] Q. Zhang, J. Xie, J. Yang and J.Y. Lee, Monodisperse icosahedral Ag, Au, and Pd nanoparticles: size control strategy and superlattice formation, ACS Nano 3 (2009) 139-148.

[35] N.G. Bastús, F. Merkoçi, J. Piella and V. Puntes, Synthesis of highly monodisperse citrate-stabilized silver nanoparticles of up to 200 nm: kinetic control and catalytic properties, Chem. Mater. 26 (2014) 2836-2846.

[36] L. Liu and A. Corma, Metal catalysts for heterogeneous catalysis: from single atoms to nanoclusters and nanoparticles, Chemical Reviews 118 (2018) 4981-5079.

[37] O.M. Wilson, M.R. Knecht, J.C. Garcia-Martinez and R.M. Crooks, Effect of Pd nanoparticle size on the catalytic hydrogenation of allyl alcohol, J. Am. Chem. Soc. 128 (2006) 4510-4511.

[38] C. Wang, G. Wang, D. van der Vliet, K. Chang, N.M. Markovic and V.R. Stamenkovic, Monodisperse Pt3Co nanoparticles as electrocatalyst: the effects of particle size and pretreatment on electrocatalytic reduction of oxygen, Phys. Chem. Chem. Phys. 12 (2010) 6933-6939.

[39] H. Vijwani, M.N. Nadagouda and S.M. Mukhopadhyay, Robust nanocatalyst membranes for degradation of atrazine in water, J. Water Process Eng. 25 (2018) 15-21.

[40] A.K. Karumuri, D.P. Oswal, H.A. Hostetler and S.M. Mukhopadhyay, Silver nanoparticles attached to porous carbon substrates: robust materials for chemical-free water disinfection, Mater. Lett. 109 (2013) 83-87.

[41] M. Yoshio, H. Wang, K. Fukuda, T. Umeno, N. Dimov and Z. Ogumi, Carbon-coated Si as a lithium-ion battery anode material, J. Electrochem. Soc. 149 (2002) A1598-1603.

[42] I.G. Gonzalez-Martinez, A. Bachmatiuk, V. Bezugly, J. Kunstmann, T. Gemming, Z. Liu, G. Cuniberti and M.H. Rümmeli, Electron-beam induced synthesis of nanostructures: a review, Nanoscale 8 (2016) 11340-11362.

[43] X. Song, Q. Yang, M. Yin, D. Tang and L. Zhou, Highly efficient pollutant removal of graphitic carbon nitride by the synergistic effect of adsorption and photocatalytic degradation, RSC Adv. 8 (2018) 7260-7268.

Acknowledgement
The authors express their gratitude to the Ministry of Education Malaysia and Tunku Abdul Rahman University College for funding this work through the Fundamental Research Grant Scheme (Grant Number 4F827) and TARUC Research Grant (Project Number 86007).

Supporting Information

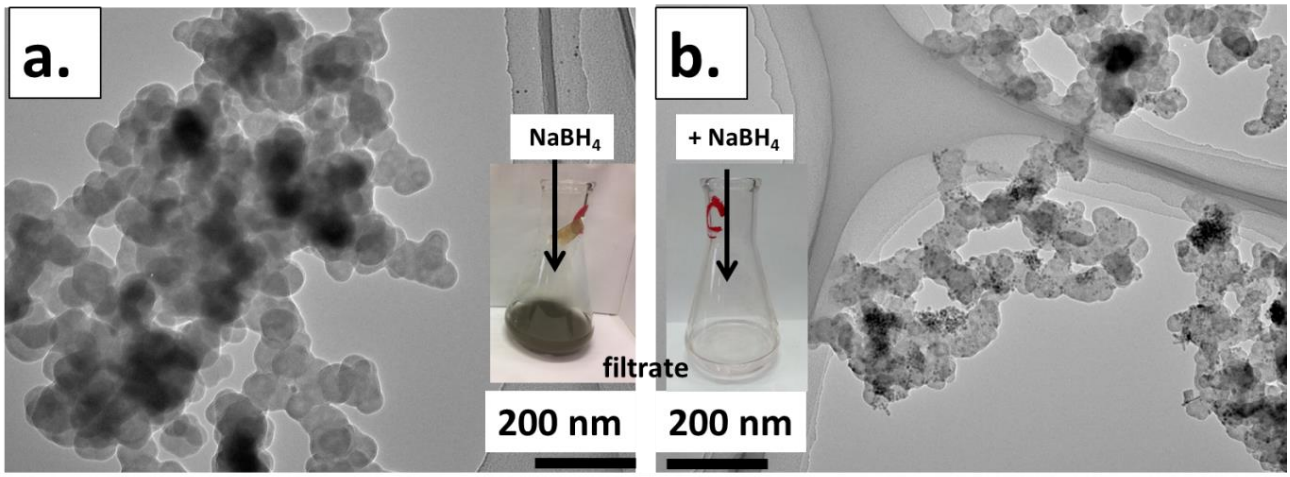

Figure S1. Bright field TEM images and photos of filtrates treated with $NaBH_4$. (a) Control experiment in which carbon without In NPs was treated with $AgNO_3$ in dark for 24 hours. The filtrate turned intensely grey indicated $NaBH_4$ reduced $AgNO_3$. (b) The colourless filtrate indicated all $AgNO_3$ reacted.

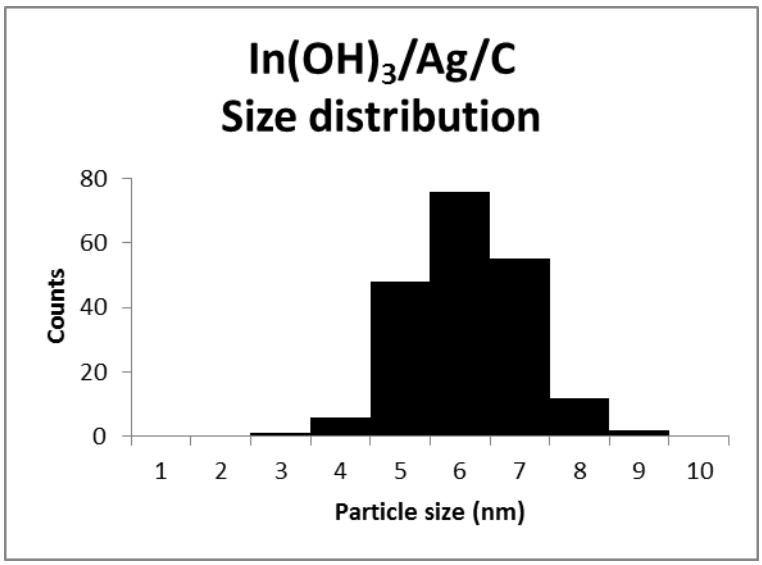

Figure S2. Size distribution of $In(OH)_3$/Ag on carbon. Only particles of similar size were observed. Based on the contrast difference alone, $In(OH)_3$/Ag could not be distinguished. PXRD showed the presence of both Ag and $In(OH)_3$ crystals.

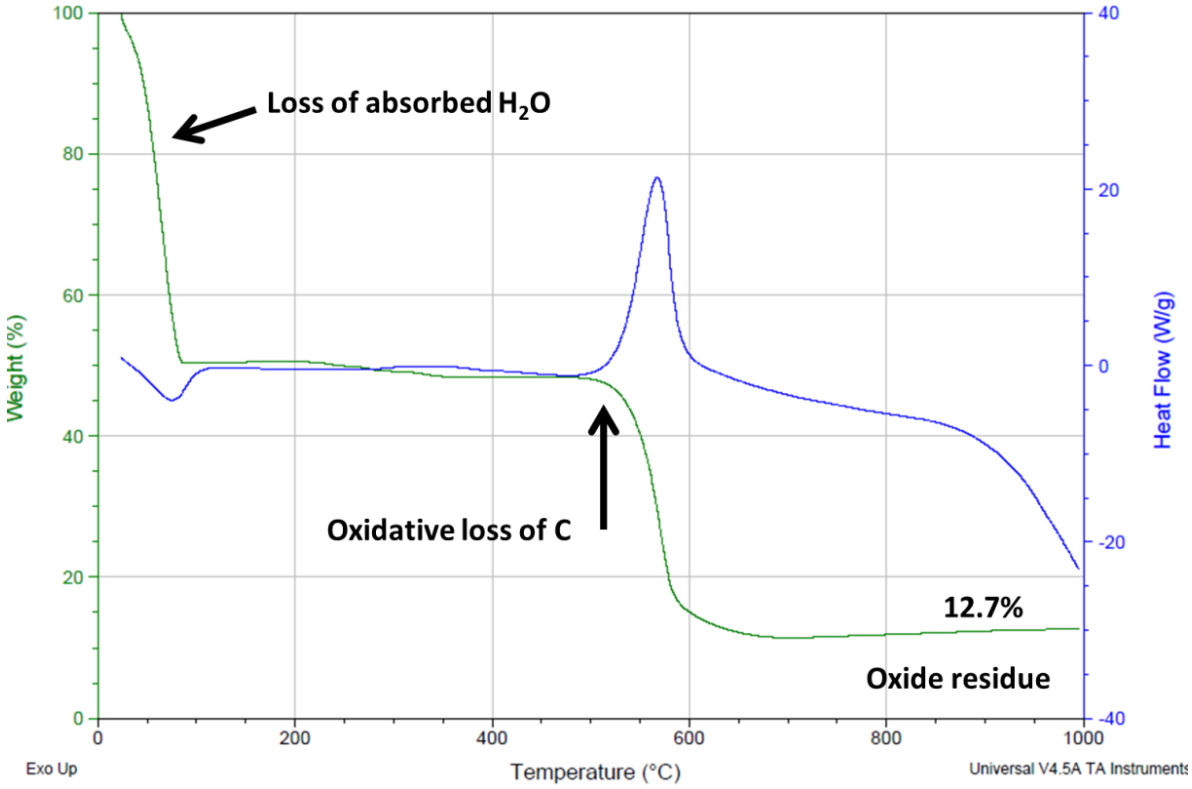

Figure S3. A thermogram of $In(OH)_3$/Ag/C composite from DSC-TGA analysis in air. Oxidative carbon loss started at 500^{o}C and a residue of 12.7% obtained at 1000 ^{o}C, indicating $In(OH)_3$/Ag loading on C was circa 13%.